Pyrolysis of Furan at Low Pressures: Vibrational Relaxation, Unimolecular Dissociation, and Incubation Times

D. Fulle, A. Dib, and J. H. Kiefer

Department of Chemical Engineering, University of Illinois at Chicago, Chicago, IL 60607

Q. Zhang, J. Yao,† and R. D. Kern*

Department of Chemistry, University of New Orleans, New Orleans, Louisiana 70148

Received: May 19, 1998; In Final Form: July 7, 1998

Vibrational relaxation, incubation times, and unimolecular dissociation of C_4H_4O have been investigated over the extended temperature range 500−3000 K in 2−5% furan−krypton mixtures, 2% furan−neon mixtures, and in pure furan. The experiments were performed in shock waves using laser-schlieren (LS) densitometry and time-of-flight (TOF) mass spectrometry. At low temperatures and low pressures, only vibrational relaxation was observed using the LS technique. This relaxation is unexpectedly slow and shows a strong nonexponential time dependence. Unimolecular dissociation is observed in TOF experiments between 1300 and 1700 K in a pressure range of 175−250 Torr as well as LS experiments between 1700 and 3000 K for pressures between 100 and 600 Torr. The TOF experiments show that under the given conditions two molecular dissociation channels leading to $C_2H_2 + CH_2CO$ or to $C_3H_4 + CO$ are dominant. The branching ratio between these channels has been determined between 1300 and 1700 K. At low temperatures, the molecular channel leading to C_3H_4 and CO is preferred, but a channel switching was observed around 1700 K. The domination of these molecular channels is consistent with the shape of the LS profiles, and these have been successfully modeled with just these two reactions. The overall unimolecular rate constant is in the falloff regime close to the low-pressure limit. By use of statistical reaction rate theory, the total unimolecular rate constant could be modeled over an extended temperature and pressure range using a value of $\langle \Delta E \rangle_{all} = 50$ cm^{-1} for the furan dissociation. In a small range of conditions at low pressures and high temperatures, both the vibrational relaxation and dissociation were resolved and incubation times estimated.

Introduction

The unimolecular dissociation of large molecules is of considerable importance in many combustion processes. Aromatic heterocycles such as furan are emitted by combustion of fuels and biomass[1] and have been identified as air pollutants.[2] Additionally, furan appears to be an excellent molecule to study the fundamentals of the unimolecular dissociation of large molecules over a wide range of conditions, covering vibrational relaxation, unimolecular dissociation, and perhaps incubation. This study describes laser-schlieren and time-of-flight experiments behind shock waves at pressures below 600 Torr that were performed over a wide temperature range. At low temperatures, only vibrational relaxation of furan was observed in diluted krypton mixtures and in the pure gas. At higher temperatures, the unimolecular dissociation becomes important. At very low pressures (<100 Torr) and higher temperatures, both processes were observed during a single experiment. From these experiments the incubation time, the delay until a steady state for the unimolecular dissociation has been achieved, could be estimated. Besides N_2O[3] and norbornene C_7H_{10},[4] furan is the only polyatomic molecule for which vibrational relaxation, unimolecular dissociation, and incubation times have been experimentally observed.

Previously, the dissociation of furan had been investigated for temperatures between 960 and 1700 K.[5−8] Grela et al.[5] performed very low pressure pyrolysis experiments and identified C_3H_4 and CO as the products of the unimolecular dissociation using mass spectrometry. The higher temperature single-pulse shock-tube (SPST) experiments[6,8] and the time-resolved infrared absorption measurements of furan disappearance[8] draw a more complicated picture of the pyrolysis mechanism. Propyne, CO, C_2H_2, CH_2CO, allene, C_4H_6, C_2H_4, CH_4, C_4H_4, C_4H_2, and benzene have been identified by gas chromatography/mass spectrometry (GC/MS) analysis. Lifshitz et al.,[6] as well as Organ and Mackie[8] suggested that the initial and rate-determining step of furan dissociation is a ring-opening process, a cleavage of the C−O bond. The resulting L-furan then reacts rapidly to form several products. This mechanism suggests that the overall rate constant for furan loss can be treated by unimolecular reaction rate theory as a rate-controlling single-channel reaction leading to L-C_4H_4O. The branching ratio between the different product channels will then depend on the energy and structure of multiple transition states. In detail, their suggested dissociation mechanism can be written as

$$C_4H_4O \rightarrow \text{L-}C_4H_4O$$

$$\rightarrow C_3H_4 + CO \qquad \Delta H_{r,298} = 110 \text{ kJ/mol} \qquad (1a)$$

$$\rightarrow CH_2CO + C_2H_2 \qquad \Delta H_{r,298} = 214 \text{ kJ/mol} \qquad (1b)$$

$$\rightarrow HCO + C_3H_3 \qquad \Delta H_{r,298} = 422 \text{ kJ/mol} \qquad (1c)$$

However, reaction 1c should be negligible because of its high heat of reaction compared to the other two channels. Its possible

† Permanent address: Department of Physics and Engineering, Xavier University of Louisiana, New Orleans, LA 70125.

S1089-5639(98)02304-4 CCC: $15.00
Published on Web 09/02/1998

contribution to the initiation of a radical chain mechanism is discussed below. It should be noticed that the heat of formation for the biradical L-furan has not been determined experimentally. Organ and Mackie[8] estimated a value of $\Delta H_{f,298\ K} = 297$ kJ/mol for L-furan and a heat of reaction of $\Delta H_{r,298} = 332$ kJ/mol for the initial dissociation step using group additivity techniques described in ref 9. This value is in good agreement with the experimental activation energies at high pressures of 324 or 327 kJ/mol[8] obtained in SPST experiments. The overall heats of reaction for the formation of final products are very well established. Because of the large variety of products, they concluded that the pyrolysis must include some contribution from a chain mechanism, which may be started by reaction 1c or by the unimolecular dissociation of either of the products C_3H_4 and CH_2CO.

The SPST studies were performed at total pressures of around 2^6 and 20 bar.[8] One would then expect that the unimolecular dissociation rate constant of a molecule the size of furan is close to the high-pressure limit. Consistent with this, there are no significant differences in the rate constants from the study at 2 bar and the study at 20 bar. The rate constant of the 2 bar study of Lifshitz et al.[6] is even a little higher than the data from the 20 bar study of Organ and Mackie, but within experimental error they agree with each other.

While the high-pressure limiting rate constant $k_{1,\infty}$ for the unimolecular furan dissociation seems to be well established, there is no information regarding falloff behavior or the low-pressure limiting rate constant. In addition, the temperature dependence of the branching ratio between the two dominant molecular channels 1a and 1b is still uncertain. Therefore, time-resolved kinetic measurements in shock waves combining the time-of-flight (TOF) and the laser-schlieren (LS) techniques are indeed helpful to improve the understanding of the pyrolysis mechanism of furan. The first low-pressure measurements of the rate constant for the initial rate-determining step (the C−O bond cleavage) and the real time measurements of major product formation are presented, giving a new measure of the branching ratio between the dissociation channels. Additionally, accurate rates at low pressures will be provided, allowing the observation of falloff effects in this reaction. Furthermore, the vibrational relaxation and incubation time measurements represent a unique opportunity to improve the understanding of collisional energy transfer and dissociation in polyatomic molecules.

Experimental Section

The details of the experimental setup for both shock tubes including the LS and TOF detection techniques have been described in previous publications.[10,11] Therefore, only relevant details of the furan dissociation experiments will be mentioned here.

Laser Schlieren. Furan was obtained from Aldrich (purity >99%) and was vacuum degassed using the middle fraction for the experiments. For the experiments in pure furan, the shock tube was directly filled with the purified vapor. Diluted mixtures of 5% and 2% furan in Kr were also prepared manometrically in a 50 L glass bulb with excimer grade krypton (Spectra gases, >99.997%). The molar refractivity of the gases was taken as a constant 6.367 for krypton and 18.432 for furan. To produce the combination of low postshock pressures and temperatures necessary for vibrational relaxation or incubation studies, various Laval nozzles were used to slow the shock wave. These nozzles are made from brass and inserted in the driven section of the shock tube close to the diaphragm. The incident shock velocity was measured by interpolation of intervals from five pressure transducers spaced about the observation window at 120 mm apart. Using thermodynamic properties of the reactants, the diluent, and the reaction products, postshock temperatures without relaxation and for fully relaxed conditions were calculated with an accuracy of ±10 K.

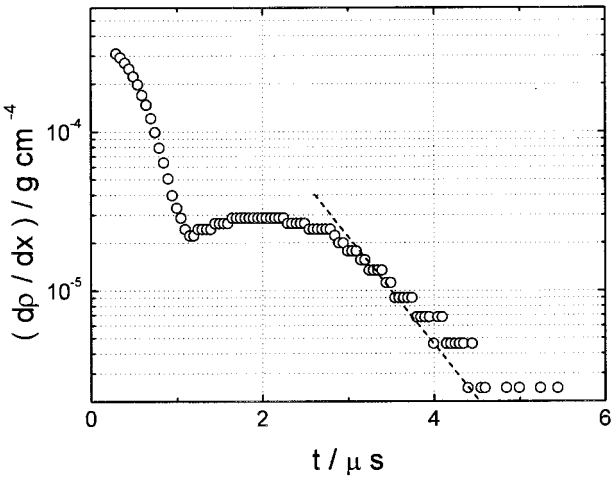

Figure 1. LS profile showing vibrational relaxation in a 2% furan/krypton mixture at $P = 68$ Torr and $T = 1168$ K. The dashed line represents the exponential fit to the final decay.

Time-of-Flight. A 2% furan−98% Ne mixture was prepared from reagents obtained from the following sources: furan from Aldrich (purity >99%) and research grade neon from Matheson (99.999%). Furan was introduced into the gas-handling system by vaporization of the liquid sample, condensed by LN_2, and doubly distilled. The middle fraction was retained for the mixture. Mass spectrometric analysis of the pure furan and of the 2% furan/neon mixture revealed an absence of impurities within the detection limit of TOF, ca. 300 ppm. The following mixtures, all with neon diluent, were prepared to determine the mass spectrometric sensitivity factors: 2% C_2H_2, 2% CO, 2% allene, 2% propyne, and 2% diketene. The calibration experiments were performed at nonreacting temperatures. For the diketene mixture, the dissociation of diketene at 1050 K occurred shortly after shock front arrival; the mass peak due to ketene, *m*/*e* 42, was constant during the observation period. The sensitivity factors for allene and propyne were found to be identical.

The temperature and pressure ranges covered by the TOF experiments are 1300−1700 K and 175−250 Torr. The mass balance is ∼100%.

Results and Discussion

Vibrational Relaxation. At temperatures below 1200 K and pressures below 100 Torr, the density gradients in the gas are solely due to vibrational relaxation. The typical semilog laser-schlieren profile of Figure 1 shows a markedly slow and nonexponential time dependence of the density gradient for mixtures of furan in krypton. The density gradients increase during the first 2 μs, reach a maximum, and then decrease exponentially after about 3 μs. In a small temperature range (503−620 K) and for total pressures around 10 Torr, we were able to resolve vibrational relaxation in pure furan (Figure 2). The vibrational relaxation is faster than that in furan/Kr mixtures, but the nonexponential time dependence of the laser-schlieren profile remains (see Table 1). Final decay times were extracted by fitting the exponential decay well after the maximum in the semilogarithmic plot. These times were corrected to Bethe−

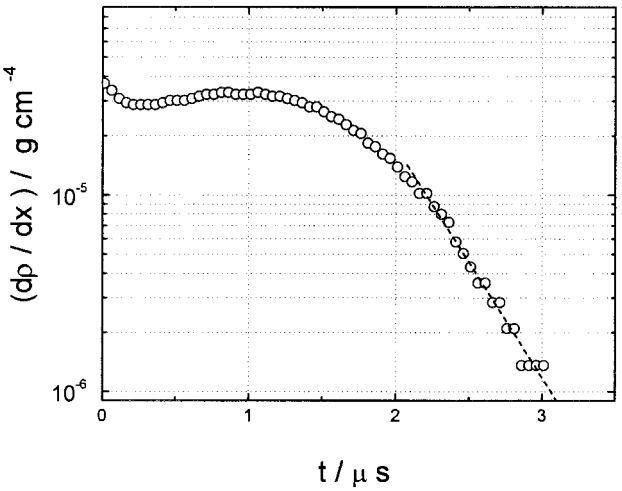

Figure 2. LS profile showing vibrational relaxation in pure furan at $P = 7$ Torr and $T = 620$ K. The dashed line represents the exponential fit to the final decay.

TABLE 1: Relaxation Times for Pure Furan and Furan/Kr Mixtures

mixture	T/K	$P\tau$/atm μs
2% furan in Kr	746	0.812
	759	0.739
	765	1.012
	840	0.438
	874	0.517
	909	0.504
	946	0.462
	982	0.457
	1034	0.476
	1102	0.357
	1168	0.299
	1294	0.179
5% furan in Kr	512	1.330
	525	1.351
	630	1.177
	637	1.087
pure furan	503	0.194
	526	0.250
	543	0.173
	549	0.190
	569	0.201
	577	0.227
	586	0.163
	587	0.169
	619	0.165
	620	0.144

Teller[12] energy relaxation times using the specification of Blythe.[13] In Figure 3 the temperature dependence of these relaxation times for diluted and pure furan is presented in a Landau−Teller plot. The measurements of $P\tau$ in pure furan, $P\tau_{\text{furan}}$, give

$$\log(P\tau_{\text{furan}}/\text{atm s}) = -8.42 + 13.9T^{-1/3} \qquad (2a)$$

From the dilute gases we are now able to calculate the $P\tau_{\text{Kr}}$ for furan infinitely diluted in Kr using a linear mixing rule. The temperature dependence can be described by

$$\log(P\tau_{\text{Kr}}/\text{atm s}) = -8.78 + 24.4T^{-1/3} \qquad (2b)$$

As the LS technique monitors the density change associated with the vibrational relaxation of furan, we compared the theoretical density change $\Delta\rho$ with the experiments. To do this, we described LS profiles for the 5% furan experiments by the

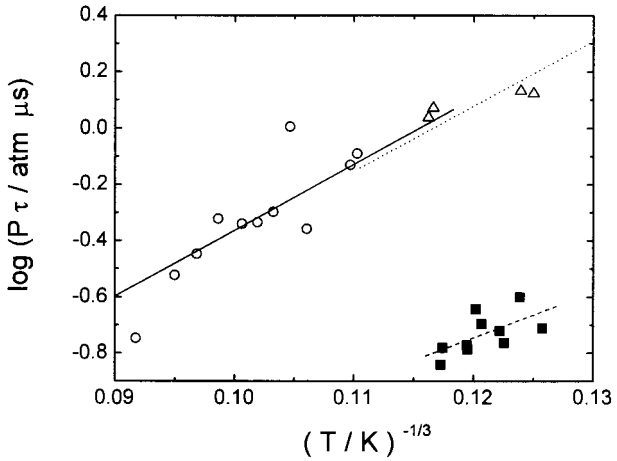

Figure 3. Landau−Teller plot for relaxation of pure furan and furan in krypton. ○, 2% furan in krypton; △, 5% furan in krypton; ■, pure furan. The solid line represents the best fit to the 2% data, the dotted line represents the best fit to the 5% data, and the dashed line represents the best fit to the pure furan data.

empirical biexponential expression

$$\frac{\mathrm{d}\rho}{\mathrm{d}x} = A\exp\left(-\frac{t}{\tau_{\text{a}}}\right) - B\exp\left(-\frac{t}{\tau_{\text{b}}}\right) \qquad (3)$$

and integrated the density gradients as

$$\Delta\rho = u_1\int_0^{\infty}\left(\frac{\mathrm{d}\rho}{\mathrm{d}x}\right)\mathrm{d}t \qquad (4)$$

The experimental density change, which was obtained by integrating the LS profile, can then be compared to the theoretical value of $\Delta\rho$. This theoretical value is calculated from thermodynamic properties as the difference between the equilibrated density and the density for the hypothetical initial state of frozen vibration but equilibrated rotation and translation. The mean absolute percent deviation is 14% compared to the experimental value. The fit of the 2% furan and the pure furan LS profiles with eq 3 was poor, and these were not integrated. Instead, we fit a single-exponential expression to the late density gradients. Using the cited temperature functions we extrapolated the $P\tau_{\text{Kr}}$ to 300 K to compare our LS data with results from ultrasonic measurements.[14] We thus obtained the average number of collisions necessary for a molecule to lose or take up one vibrational quantum for furan, $Z_{10} = 760$. The value of Z_{10} can be correlated (Lambert−Slater plot[14]) to the lowest vibrational mode of the molecule. For furan, the frequency of this lowest vibrational mode is $\nu_{\text{min}} = 603$ cm^{-1}.[15] Lambert and Slater[14] give values between $Z_{10} = 100$ and $Z_{10} = 200$ for a molecule with two or more hydrogen atoms and a lowest vibrational frequency of 600 cm^{-1}.

The complex relaxation exhibited here by furan and by other large molecules (see, for example, ref 16), can only be understood by a detailed master-equation analysis, which will be presented together with more examples in upcoming papers.

Unimolecular Dissociation. Whereas both of the earlier single-pulse shock-tube experiments[6,8] identified several pyrolysis products as mentioned in the Introduction, the TOF experiments reported herein detected only major products, which result directly from reactions 1a and 1b. Example concentration profiles for the products and reactants are displayed in Figure 4. No other products were detected during the observation period of ~800 μs. The branching ratio for reaction 1b/1a was determined by measuring the ratio $[C_2H_2]/[CO]$ at the end of

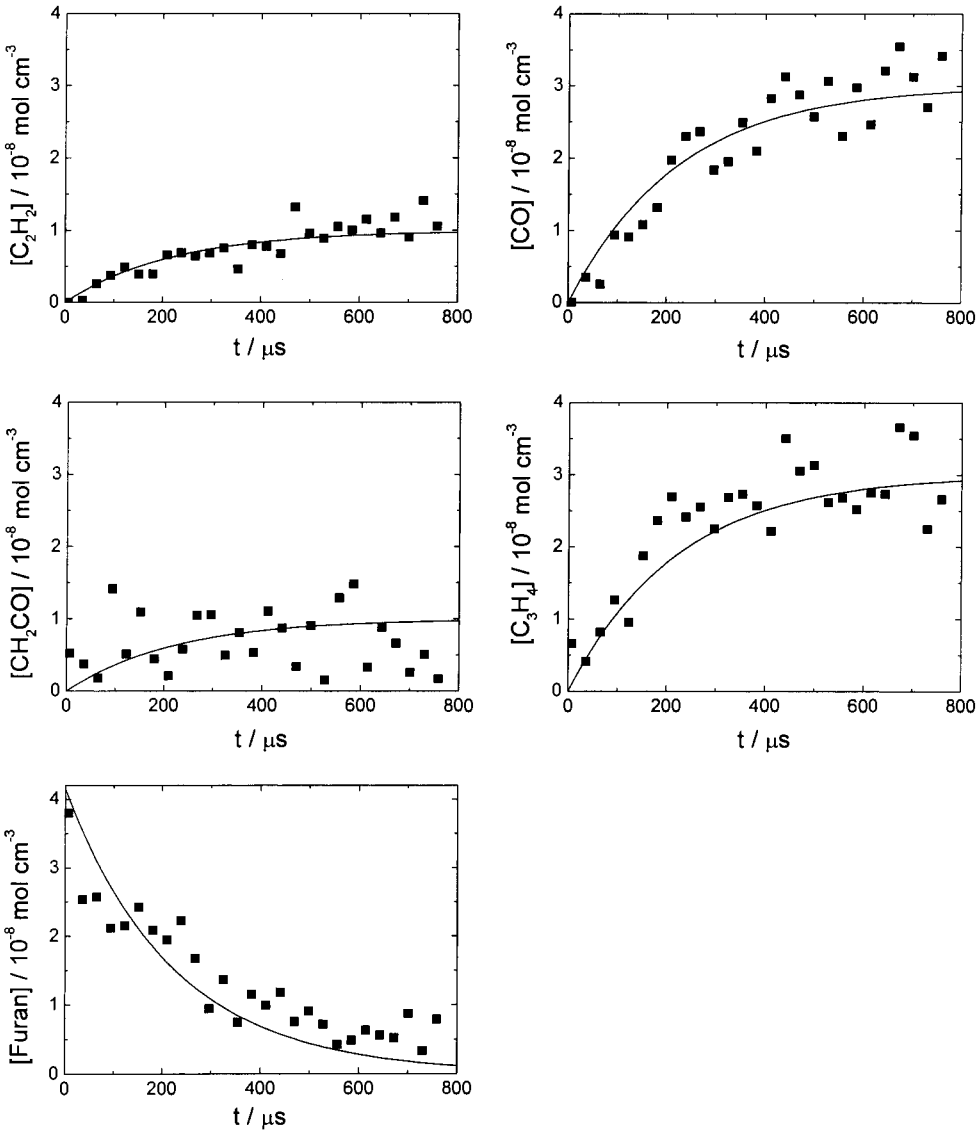

Figure 4. TOF concentration profiles in 2% C_4H_4O/98% Ne at 1533 K and 198 Torr. The solid lines are calculated from the model using reactions 1a and 1b only.

the observation period. The temperature dependence of the branching ratio is shown in Figure 5. The data can be fitted by the following expression:

$$[C_2H_2]/[CO] = (5.5 \times 10^{-9})T^{2.5} \qquad (5)$$

Some earlier points in the temperature range 1060−1260 K[6] were also included in this fit.

The second set of laser-schlieren experiments, with higher temperatures, now show density gradients due to the unimolecular dissociation of furan. These LS experiments cover a wide range of experimental conditions: 1700−2500 K at pressures between 100 and 600 Torr. Similar to the TOF experiments, these LS profiles can accurately be modeled with just the initial reaction 1a and 1b. Figure 6 shows two examples of laser-schlieren time profiles together with this model calculation. For this model, the heats of formation, vibrational frequencies, and moments of inertia for product species were taken from the literature.[17,18] For furan, vibrational frequencies and the molecular geometry needed to calculate the moments of inertia were taken from an ab initio calculation by Montero et al.,[15] whose calculated molecular parameters agree very well with earlier experimental results.[19] The rate constants k_1 obtained from LS experiments are shown in an Arrhenius representation (Figure 7).

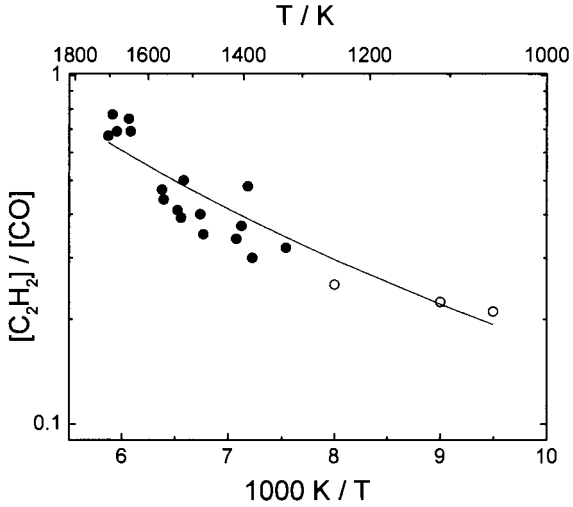

Figure 5. The branching ratio k_{1b}/k_{1a}, [C2H2]/[CO], vs temperature: ●, TOF results; ○, SPST results. $[C_2H_2]/[C_3H_4]$ is in the range 1060−1260 K.[6] Solid line represents an empirical fit to the data.

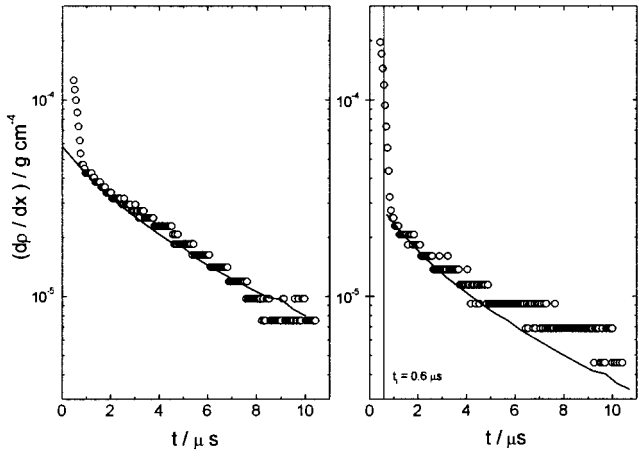

Figure 6. LS profiles showing unimolecular dissociation of 2% furan in krypton at $P = 596$ Torr and $T = 1834$ K (left trace) and at $P = 261$ Torr and $T = 1963$ K including an incubation time of 0.6 μs (right trace). The solid lines represent the kinetic model using reactions 1a and 1b.

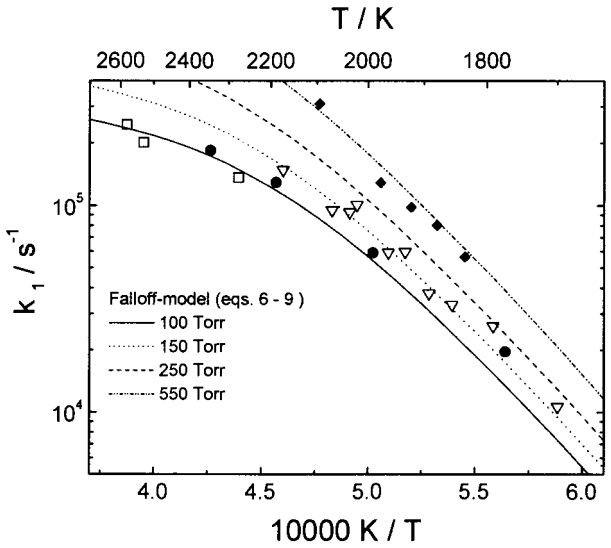

Figure 7. Arrhenius representation of the unimolecular rate constant k_1 derived from LS experiments without chain reaction: □, 100 Torr; ●, 150 Torr; ▽, 250 Torr; ◆, 550 Torr. The lines represent the falloff model (eq 6) with $k_{1,0}$, $k_{1,\infty}$, and $F_{1,\text{cent}}$ from eqs 7−9.

As already mentioned, Lifshitz et al.[6] as well as Organ and Mackie[8] found several products clearly indicating a chain reaction under their experimental conditions. The LS experiments are performed on a 10 μs time scale, while the reaction times for the SPST experiments are ca. 300 μs[8] or even 2 ms.[6] Therefore, under our conditions, the LS profiles are only weakly sensitive to chain reaction when compared to the SPST studies; the chain does not have time to develop.

The source of radicals needed for the chain so evident in single-pulse experiments is not clear. Organ and Mackie[8] suggested reaction 1c, but this has serious problems, especially at low temperatures. To reach HCO and propargyl from the L-furan intermediate requires a prior 1,2 shift to either O═CH−CH═C═CH_2 or O═CH−CH_2−C≡CH, quite stable species not easily dissociated or detected in the single-pulse studies. At high temperatures, dissociation of the dominant products C_3H_4 and CH_2CO is a likely possibility. At the lowest temperatures impurity initiation should at least be considered.

Under special conditions of very low pressure, the density gradient could only be modeled by introducing an incubation time t_i (see refs 4 and 20). This incubation is the delay preceding steady-state dissociation. In some laser-schlieren signals we were able to resolve both vibrational relaxation and unimolecular dissociation, which allows the estimation of an incubation time. However, in most of the dissociation experiments the signal generated by the vibrational relaxation of furan is hidden under the shock front signal. The incubation times will be discussed later; for now we will concentrate on the steady unimolecular reaction rate for furan dissociation.

While Lifshitz et al.[6] found almost no temperature dependence to the branching ratio between reactions 1 at temperatures below 1300 K, the TOF experiments from this study show a weak temperature dependence of this branching ratio for temperatures above 1400 K. The TOF branching ratio, given in eq 5, was used to model the laser-schlieren profiles at high temperatures.

It was suggested that furan dissociation occurs via a biradical mechanism.[6,8] The initial and rate-determining step of the unimolecular dissociation of furan is then a cleavage of the C−O bond leading to a stabilized biradical, L-furan. This biradical further fissions either to C_2H_2 + CH_2CO or to C_3H_4 + CO, where the latter requires an H atom shift. While the overall rate constant k_1 depends only on the rate-determining initial step, the temperature dependence of the branching ratio strongly depends on the threshold energies and the properties of the transition states between L-furan and the final products. One can also imagine an alternative reaction pathway starting with an H atom shift from C1 to C2 in furan followed by direct dissociation into the products propyne, ketene, acetylene, and CO, as proposed by Higgins et al.[21] In this mechanism, no biradical is formed intermediately, but the *A*-factor of the high-pressure limit A_∞ for an H atom shift should be on the order of $10^{13}-10^{14}$ s^{-1}. Both single-pulse shock-tube experiments, which have been performed close to the high-pressure limit for the unimolecular dissociation of furan, derive an *A*-factor of 2.5×10^{15} s^{-1}. This *A*-factor is thus consistent with the rate-controlling formation of a biradical intermediate from an initial CO bond cleavage. The high-pressure activation energy $E_{A,\infty}$ observed in both SPST studies, which is in good agreement with the CO bond energy for the ring opening, strongly supports this notion of a biradical mechanism.

For modeling of the LS profiles, we interpret the experimental rate constant as determined by the initial CO bond cleavage. The following procedure has then been used to construct an RRKM model of this process. The overall rate constant k_1 derived from the two SPST studies, which agree very well with each other, was taken as the high-pressure limiting rate constant $k_{1,\infty}$. The low-pressure limiting rate constant $k_{1,0}$ was calculated following Troe.[22] As the low-pressure limit k_0 for strong collisions does not depend on properties of the products and only slightly depends on the chosen structure of the transition state, the calculation is straightforward using the well-established[15,19] molecular properties of furan. We used a value of 27 400 cm^{-1} (327 kJ/mol) as the threshold energy for the CO bond cleavage, which is consistent with the apparent activation energy at high-pressure $E_{a,\infty}$ from refs 6 and 8. This value for ϵ_0 is also consistent with estimations of the heat of formation for L-furan using group additivity techniques. The collision efficiency β_c was derived from a fixed $-\langle\Delta E\rangle_{all}$, and this was adjusted to fit the experimental data from the LS experiments. We found good agreement using a temperature-independent and rather routine value of $-\langle\Delta E\rangle_{all} = 50$ cm^{-1}.[20] This value corresponds to a collision efficiency of $\beta_c = 0.039$ and $\langle\Delta E\rangle_{down} = 250$ cm^{-1} at 1000 K and $\beta_c = 3.5 \times 10^{-3}$ and $\langle\Delta E\rangle_{down} = 820$ cm^{-1} at 3000 K. These values were used to calculate broadening factors F_{cent}, modeling the falloff behavior

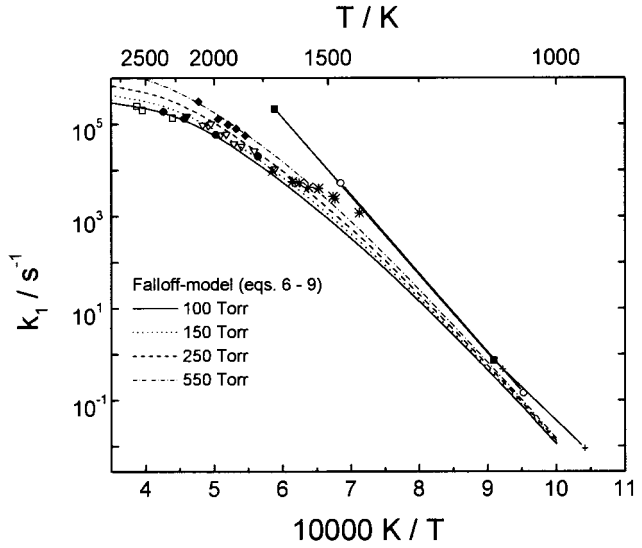

Figure 8. Arrhenius representation of the unimolecular rate constant k_1 with □, 100 Torr (LS); ●, 150 Torr (LS); ▽, 250 Torr (LS); ◆, 550 Torr (LS); *, 150−250 Torr (TOF) from this work and −○−, ref 6; −■−, ref 8; −+−, ref 7. The lines represent the falloff model (eq 6) with $k_{1,0}$, $k_{1,\infty}$, and $F_{1,\text{cent}}$ from eqs 7−9.

of the unimolecular dissociation as described in ref 22. The adjusted $-\langle\Delta E\rangle_{\text{all}}$ value strongly depends on the chosen threshold energy, because a change in the threshold energy directly affects the strong collision low-pressure limiting rate constant. Nonetheless, a consistent model to describe the pressure and temperature dependence of the furan dissociation rate constant has been developed. This model will need to be refined, when more details about the potential-energy surface, especially the energetics of the intermediate, L-furan, are available. From the LS data, the pressure dependence of the rate constant $k_1 = k_{1a} + k_{1b}$ at fixed temperature can be described by[23]

$$k_1 = \frac{k_{1,0}[\text{M}]}{1 + k_{1,0}[\text{M}]/k_{1,\infty}} \times F\left(1 + \left(\frac{\log(k_{1,0}[\text{M}]/k_{1,\infty})}{N - 0.14(\log(k_{1,0}[\text{M}]/k_{1,\infty}) + c)}\right)^2\right)^{-1} \quad (6)$$

where $c = -0.4 - 0.67 \log F_{1,\text{cent}}$ and $N = 0.75 - 1.27 \log F_{1,\text{cent}}$.

Using the following temperature dependencies for the parameters $k_{1,\infty}$, $k_{1,0}$, and $F_{1,\text{cent}}$,

$$k_{1,\infty} = 2 \times 10^{15} \exp(-39\,632K/T)\ \text{s}^{-1} \quad (7)$$

$$k_{1,0}/[\text{Kr}] = 2.8 \times 10^{59}\,(T/\text{K})^{-11.9} \times \exp(-39\,380K/T)\ \text{cm}^3\ \text{mol}^{-1}\ \text{s}^{-1} \quad (8)$$

$$F_{1,\text{cent}} = \exp(-5208\ \text{K}/T) + \exp(-T/594K) \quad (9)$$

the rate constant can be well described over an extended temperature and pressure range. In Figure 7, the rate constants from the LS experiments alone are presented divided into four narrow groups according to the postshock pressure. The lines represent the RRKM rate constants at constant pressures of 100, 150, 250, and 550 Torr, respectively, as described by eq 6 with the temperature dependence of $k_{1,\infty}$, $k_{1,0}$, and F_{cent} from eqs 7−9.

In Figure 8 the TOF and LS experimental rate constants are presented in an Arrhenius representation together with the modeled falloff behavior and the literature results[5,6−8] over a wider temperature regime. While the SPST data are close to the high-pressure limit, a strong falloff of the LS rate constants at low pressures and high temperatures was observed. Whereas the high-temperature rates are close to this falloff model and the LS results, at the lowest temperatures the TOF rates are above the model prediction. Since the falloff model can describe the LS profiles with a reasonable value of $-\langle\Delta E\rangle_{\text{all}} = 50\ \text{cm}^{-1}$ as well as the high-pressure data from refs 6 and 8, we have no explanation for this low-temperature discrepancy.

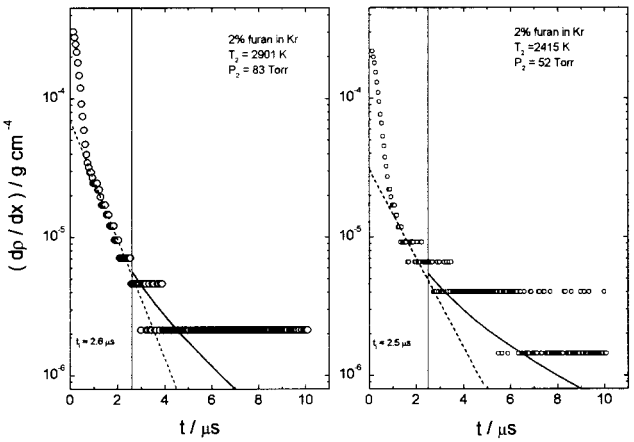

Figure 9. LS profiles showing relaxation and unimolecular dissociation of furan. The dashed lines represent the exponential fit to the density gradients due to vibrational relaxation. The solid lines represent the kinetic model using the unimolecular dissociation reaction 1a,b.

Incubation Times. Under special conditions, both vibrational relaxation and unimolecular dissociation can be seen in the LS profiles and incubation times can then be estimated. Two LS profiles, which appear to show both processes, are given in Figure 9. The first exponential decay is due to the vibrational relaxation; after a few microseconds the slope changes as the unimolecular dissociation begins. Such profiles, which show both processes, were not used to evaluate dissociation rate constants because of the great uncertainty in time origin, but the rate constants derived from these experiments are fully consistent with the profiles showing only dissociation.

The experimental conditions under which both relaxation and dissociation can be resolved are very narrow. The pressure has to be low enough so the vibrational relaxation time is on the order of a few microseconds. But low pressure decreases the rate of the dissociation process, which is then close to the low-pressure limit. Therefore, the temperature has to be increased to compensate. As a result, we were only able to resolve both processes at pressures below 100 Torr and temperatures above 2000 K. As mentioned previously, incubation times could also be estimated from the experiments where the schlieren profile shows dissociation only. Vibrational relaxation is very fast, so the density gradients from this are covered by the shock-front signal and are not seen. Nonetheless, to accurately model the experiments, a short incubation time has to be introduced to reproduce the measured density gradients (see Table 2).

All measured incubation times are plotted as the ratio t_i/τ vs temperature in Figure 10. The relaxation time τ was extrapolated from measurements at low temperatures using the Landau−Teller expression given before. The ratio is about 5 around 1700 K and rises slightly to 8 at 2500 K. These ratios are little higher than what has been observed for the norbornene dissociation,[4] where ratios between 2.5 and 5 have been extracted from laser-schlieren experiments.

Incubation times have also been estimated from N_2O dissociation experiments using the LS technique.[3] While vibra-

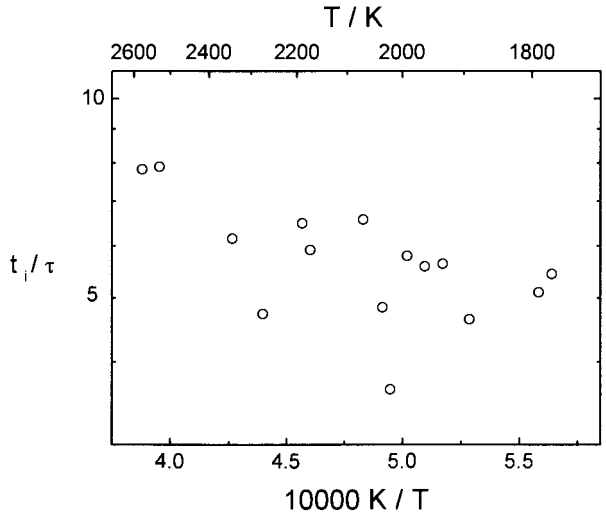

Figure 10. Incubation times for furan dissociation

TABLE 2: Experimental Data for Furan Dissociation (Induction Times Are in Laboratory Time)

T_2/K	P_2/Torr	$k_1/10^4$ s^{-1}	k_{1a}/k_{1b}	t_i/μs
1700	306	1.07	1.41	0
1773	182	1.96	1.17	1.0
1791	280	2.61	1.12	0.6
1834	596	5.66	1.58	0
1854	283	3.31	0.95	0
1879	591	8.02	0.63	0
1892	276	3.76	0.85	0.5
1922	564	9.82	0.63	0
1934	270	5.98	0.78	0.6
1977	533	12.9	0.63	0
1963	262	5.92	0.72	0.6
1991	159	5.90	0.71	1.0
2021	243	10.1	0.62	0.4
2035	282	9.28	0.59	0.5
2070	240	9.48	0.53	0.7
2096	510	31.0	0.63	0
2174	234	9.34	0.40	0.6
2189	152	12.9	0.40	1.0
2276	94	13.6	0.32	1.1
2346	129	18.4	0.20	1.0
2529	105	20.1	0.20	1.4
2578	109	24.5	0.20	1.3

tional relaxation and unimolecular dissociation are observed in a single LS profile in the furan and norbornene experiments, the N_2O incubation times could only be estimated, because the incubation period was shorter than 1 μs and, therefore, hidden behind the shock-front signal.

Acknowledgment. This research was supported by the U.S. Department of Energy, Office of Basic Energy Science, under Contracts DE-FG02-85ER13384 (J.H.K.) and DE-FG05-85ER13400 (R.D.K.). D.F. thanks the Deutsche Forschungsgemeinschaft for a postdoctoral fellowship.

References and Notes

(1) Graedel, T. E.; Hawkins, D. T.; Claxton, L. D. *Atmospheric Chemical Compounds: Sources, Occurrence, and Bioassay*; Academic Press: New York, 1986.

(2) Pelliziari, E. D.; Bunch, J. D.; Berkeley, R. E.; McRae, J. *Anal. Chem.* **1976**, *48*, 803.

(3) Dove, J. E.; Nip, W. S.; Teitelbaum, H. In *Proceedings of the 15th International Symposium on Combustion*; The Combustion Institute: Pittsburgh, 1974; p 903.

(4) Kiefer, J. H.; Kumaran, S. S.; Sundaram, S. *J. Chem. Phys.* **1993**, *99*, 3531.

(5) Grela, M. A.; Amorebieta, V. T.; Colussi, A. J. *J. Phys. Chem.* **1985**, *89*, 38.

(6) Lifshitz, A.; Bidani, M.; Bidani, S. *J. Phys. Chem.* **1986**, *90*, 5373.

(7) Bruinsma, O. S. L.; Tromp, P. J. J.; de Sauvage Nolting, H. J. J.; Moulijn, J. A. *Fuel* **1988**, *67*, 334.

(8) Organ, P. P.; Mackie, J. C. *J. Chem. Soc., Faraday Trans.* **1991**, *87*, 815.

(9) Benson, S. W. *Thermochemical Kinetics*, 2nd ed.; Wiley: New York, 1976.

(10) Kiefer, J. H.; Manson, A. C. *Rev. Sci. Instrum.* **1981**, *52*, 1392.

(11) Kiefer, J. H.; Zhang, Q.; Kern, R. D.; Chen, H.; Yao, J.; Jursic, B. S. In *Proceedings of the 26th International Symposium on Combustion*; The Combustion Institute: Pittsburgh, 1996; Vol. I, p 651.

(12) Cottrell, T. L.; McCoubrey, J. C. *Molecular Energy Transfer in Gases*; Butterworths: London, 1961.

(13) Blythe, P. A. *J. Fluid Mech.* **1961**, *10*, 33.

(14) Lambert, J. D.; Slater, R. *Proc. R. Soc. London, Ser. A* **1959**, *253*, 277.

(15) Montero, L. A.; Gonzalez-Jonte, R.; Diaz, L. A.; Alvarez-Idaboy, J. R. *J. Phys. Chem.* **1994**, *98*, 5607.

(16) Kiefer, J. H.; Sathyanarayama, R. *Int. J. Chem. Kinet.* **1997**, *29*, 705.

(17) *JANAF Thermodynamic Tables*, No. 14; Natl. Stabd. Ref. Data Ser.; National Bureau of Standards, 1985.

(18) Burcat, A.; McBride, B. *1995 Ideal Gas Thermodynamic Data for Combustion and Air-Pollution Use*, TAE report No. 732; Technion: Haifa.

(19) (a) Bak, B.; Christensen, D.; Dixon, W. B.; Hansen-Nygaard, L.; Rastrup-Anderson, J.; Schotlander, M. *J. Mol. Spectrosc.* **1962**, *9*, 124. (b) Rico, M.; Barrachina, M.; Orza, J. M. *J. Mol. Spectrosc.* **1967**, *24*, 133.

(20) Tsang, W.; Kiefer, J. H. In *The Chemical Dynamics and Kinetics of Small Radicals*; Liu, K., Wagner, A. F., Eds.; World Scientific: Singapore, Chapter 3, 1995; p 58.

(21) Higgins, J.; Zhou, X.; Liu, R. *J. Phys. Chem.* **1997**, *101*, 7231.

(22) (a) Troe, J. *J. Chem. Phys.* **1977**, *66*, 4745. (b) Troe, J. *J. Chem. Phys.* **1977**, *66*, 4748.

(23) (a) Troe, J. *Ber. Bunsen-Ges. Phys. Chem.* **1983**, *87*, 161. (b) Gilbert, R. G.; Luther, K.; Troe, J. *Ber. Bunsen-Ges. Phys. Chem.* **1983**, *87*, 161.